Supporting Information

Coordination chemistry-driven dynamic crosslinked hydrogel platform with ROS/pH responsiveness and photothermal activity for osteoporotic bone defect repair

Zhiqiang Yang[#1], Yufan Zhu[#2], Han Yu[#3], Lin Cai[*1], Ping Wu[*4], Xiaozhen Lu[*5], Minhao Wu[*1]

[1] Department of Spine Surgery and Musculoskeletal Tumor, Zhongnan Hospital of Wuhan University, 168 Donghu Street, Wuchang District, Wuhan 430071 Hubei, People's Republic of China

[2] Department of Radiation and Medical Oncology, Zhongnan Hospital, Wuhan University, Wuhan, China

[3] Department of Pathology, Hubei Provincial Clinical Research Center for Accurate Fetus Malformation Diagnosis, Key Laboratory of Zebrafish Modeling and Drug Screening for Human Diseases of Xiangyang City, Xiangyang No.1 People's Hospital, Hubei University of Medicine, Xiangyang, 441000, China

[4] State Key Laboratory of Macromolecular Drugs and Large-scale Preparation, School of Pharmaceutical Science, Wenzhou Medical University, Wenzhou 325035, China

[5] Department of Emergency, Ningbo No.2 Hospital, Wenzhou Medical University, Ningbo, 315010, China

[#] These authors contributed equally to this work

* Correspondence should be addressed to:

Dr. Minhao Wu. Email: wuminhao1991@whu.edu.cn

Department of Spine Surgery and Musculoskeletal Tumor, Zhongnan Hospital of Wuhan University, 168 Donghu Street, Wuchang District, Wuhan 430071 Hubei, People's Republic of China

Dr. Xiaozhen Lu. Email: nblxzh@hotmail.com

Department of Emergency, Ningbo No.2 Hospital, Wenzhou Medical University, Ningbo, 315010, China

Dr. Ping Wu. Email: wuping@wmu.edu.cn

State Key Laboratory of Macromolecular Drugs and Large-scale Preparation, School of Pharmaceutical Science, Wenzhou Medical University, Wenzhou 325035, China

Dr. Lin Cai. Email: orthopedics@whu.edu.cn

Department of Spine Surgery and Musculoskeletal Tumor, Zhongnan Hospital of Wuhan University, 168 Donghu Street, Wuchang District, Wuhan 430071 Hubei, People's Republic of China

Supplementary experimental section

1. Materials and methods

1.1. Materials

Sodium alginate (Alg), hyaluronic acid (HA), tannic acid (TA), sodium hydroxide (NaOH), 4′-6-diamidino-2-phenylindole (DAPI), and Triton X-100 were purchased from Sigma-Aldrich Trading Co., Ltd. (Shanghai, China). 3,4-dihydroxyphenylalanine, 3-aminobenzeneboronic acid, 1-Ethyl-3-(3-dimethylaminopropyl) carbodiimide (EDC), and N-hydroxysuccinimide (NHS) were purchased from Macklin Biochemical Technology Co., Ltd. (Shanghai, China). 1,1-Diphenyl-2-picrylhydrazyl (DPPH), 2,2′-azinobis (3-ethyl benzothiazoline-6-sulfonic acid) (ABTS), and hydrogen peroxide (H_2O_2) were obtained from Aladdin Chemistry Co., Ltd. (Shanghai, China). (Nanjing, China). Lipopolysaccharide (LPS) was purchased from Med Chem Express (Monmouth Junction, NJ, USA). Fetal bovine serum (FBS), Dulbecco's modified Eagle's medium (DMEM), alpha-modified Eagle's medium (α-MEM), phosphate-buffered saline (PBS), trypsin-EDTA (0.25%), and penicillin/streptomycin (P/S) were purchased from Gibco (Grand Island, USA). Mouse calvaria-derived MC3T3-E1 pre-osteoblastic cells, human umbilical vein endothelial cells (HUVECs), and macrophages (RAW264.7 cells) were obtained from the Institute of Biochemistry and Cell Biology of the Chinese Academy of Sciences (Shanghai, China). Mouse bone marrow-derived mesenchymal stem cells (BMSCs) and osteogenic induction medium were sourced from Cyagen Biosciences Inc. (Guangzhou, China). Cell Counting Kit-8 (CCK-8), live/dead cell staining kit, dihydroethidium (DHE), and 2',7'-dichlorofluorescin diacetate (DCFH-DA) were purchased from BestBio Biotechnologies (Shanghai, China). The TRIzol RNA extraction kit, radioimmunoprecipitation assay (RIPA) lysis buffer, 5-bromo-4-chloro-3-indolyl phosphate/nitro blue tetrazolium (BCIP/NBT) alkaline phosphatase (ALP) color development kit, Hoechst 33342, BeyoClick™ 5-ethynyl-2 deoxyuridine (EdU)-555 imaging kit, bicinchoninic acid (BCA) protein assay kit, 5,5′,6,6′-tetrachloro-1,1′,3,3′-tetraethyl-imidacarbocyanine iodide (JC-1) staining assay kit, and lipid peroxidation malondialdehyde (MDA) assay kit were obtained from Beyotime Biotechnology (Shanghai, China). Alizarin red S (ARS) staining kit and Von Kossa staining kit were obtained from Solarbio Co., Ltd. (Beijing, China). All reagents were analytically pure and used without any further treatment.

1.2. Synthesis and characterization of CM, TCM, HA-DOPA, and Alg-PBA

For the preparation of CM, 2 g of $CaCl_2$ was dispersed in 5 mL of deionized (DI) water under vigorous stirring until complete dissolution. Next, the as-prepared $CaCl_2$ solution was slowly injected into the Na_2CO_3 solution using a syringe pump (flow rate: 0.2 mL/min) under magnetic stirring (800 rpm). Ultimately, the resulting white product, CM, was collected via centrifugation and washed thoroughly. Furthermore, the TCM was fabricated by the polyphenol-assisted coordination chemistry method reported in the previous study. In brief, 500 mg TA was dissolved in 50 mL NaOH (0.05 M) solution and stirred for 30 min. Then, the obtained CM (100 mg) was introduced into the mixture above and stirred for 15 min. Finally, the suspension was transferred to the Teflon-lined autoclave and heated to 180°C for 6 h. After naturally cooling to room temperature, the TCM product, characterized by a color change from white to brown, was collected by centrifugation and washed with ethanol and DI water three times each.

HA-DOPA was prepared according to the literature, with minor modifications[1]. Briefly, HA (2 g) was added to 400 mL of DI water and stirred vigorously until completely dissolved, resulting in a high-viscosity solution. Simultaneously, DOPA (0.2 g) was added to the mixture and thoroughly mixed in the dark, followed by the addition of EDC (0.24 g) and NHS (0.24 g), and the pH was adjusted to 5.5. The reaction mixture was stirred at room temperature for an additional 6 h. The resulting product was dialyzed against DI water using a dialysis membrane, then lyophilized. Following modifications of previous protocols, Alg-PBA was synthesized. Briefly, Alg (1.0 g) and 3-aminophenylboronic acid (0.55 g) were dissolved in DI water (100 mL). Next, EDC (0.76 g) and NHS (0.46 g) were sequentially added to the above mixture, which was stirred for 24 h. Finally, the solution was transferred to a dialysis bag, dialyzed in DI water for 4 days, and then freeze-dried for further use.

The morphologies and microstructures of various materials were characterized using a field-emission scanning electron microscope (FE-SEM, Zeiss, SIGMA, Germany) equipped with an energy-dispersive spectrometer (EDS). The phase structure composition of various materials was detected by proton-1 nuclear magnetic resonance (^{1}H-NMR, AV500 MHz, Bruker, Switzerland), X-ray photoelectron spectroscopy (XPS, ESCALAB 250XI, Thermo Scientific, New York), X-ray diffraction (XRD, Ultima4, Japan), and Fourier transform infrared spectroscopy (FTIR, Nicolet 6700, Thermo Fisher Scientific, USA). The ultraviolet-visible-near-infrared (UV-vis-NIR) absorption spectroscopy of various materials was performed using a UV-vis spectrophotometer (U-3010, Hitachi, Japan). The contact angle measuring instrument (Lauda Scientific LSA100, Germany) was used to record the water contact angle of the samples. Thermogravimetric analysis (TGA) was conducted on a TG209F1 (Netzsch, Germany) under N_2 atmosphere. To quantify Ca2+ release, the samples were soaked in Tris-HCl buffer (pH 7.4) at 37°C under gentle shaking (100 rpm). The resulting solutions were analyzed using an inductively coupled plasma optical

emission spectrometer (ICP-OES, Optima 7000 DV, USA). During immersion, the solution pH was monitored with a pH meter (FE28-Standard, Mettler Toledo, Shanghai, China).

1.3. Biological activity of functionalized microspheres

The cytotoxicity of functionalized microspheres was assessed using the CCK-8 assay. Both BMSCs and RAW264.7 cells were cocultured with various concentrations of CM or TCM (0, 0.125, 0.25, 0.5, and 1 mg/mL) for 3 days. The absorbance of the cell supernatant in the different treatment groups was measured at 450 nm using a microplate reader. To evaluate osteogenic activity, BMSCs were cultured with extracts prepared by incubating CM and TCM with osteogenic induction medium. After 7 days of induction, ALP staining and activity assay were performed using a BCIP/NBT color development kit and an ALP activity assay kit according to the manufacturer's instructions. After 14 days of induction, the fixed samples were stained with ARS solution, followed by three washes with PBS. For quantification, the samples were treated with a 10% cetylpyridinium chloride solution to elute the dye, and absorbance was determined at 562 nm. Images were captured using an optical microscope. For quantitative real-time polymerase chain reaction (qRT-PCR) analysis, cells from different treatment groups were collected, and total RNA was extracted using TRIzol reagent according to the manufacturer's instructions. After reverse transcription, qRT-PCR was performed on a 7500 Real-Time PCR system (Applied Biosystems, USA) using ChamQ SYBR qPCR Master Mix according to the manufacturer's instructions. The expression levels of the target genes were quantified using the $2^{-\Delta\Delta CT}$ method, normalized to the reference gene GAPDH. Primers used in this study are listed in **Table S1**. For immunofluorescence staining, cells were fixed with 4% paraformaldehyde for 30 min at 4°C, permeabilized with 0.1% Triton X-100 for 10 min, and blocked with goat serum for 25 min. After washing three times with PBS, the cells were incubated with primary monoclonal antibodies against Col-1 and OPN at 4°C. After removing the primary antibodies, the cells were incubated in the dark with the corresponding secondary antibodies for 1 h. Subsequently, the cell nuclei were stained with DAPI. The cells were photographed under an inverted fluorescence microscope.

The intracellular ROS-scavenging ability of the microspheres was tested using RAW264.7 cells. Briefly, cells were seeded in a 24-well plate for 24 h and incubated with various samples in an oxidative environment (500 μM H_2O_2). After 24 h incubation, cells were then incubated with DCFH-DA (10 μM) for 15 min. After that, the cells were imaged with an inverted fluorescent microscope and analyzed for intracellular ROS production using a flow cytometer (CytoFLEX, Beckman Coulter, USA).

For the evaluation of anti-inflammatory activity, RAW264.7 cells were incubated with LPS (1 μg/mL) for 12 h, after which they were treated with or without various samples for another 3 days. For immunofluorescence staining, cells were fixed with 4%

paraformaldehyde for 30 min at 4°C, permeabilized with 0.1% Triton X-100 for 10 min, and blocked with goat serum for 25 min. After washing three times with PBS, the cells were incubated with primary monoclonal antibodies against F4/80, CD86, and CD206 at 4°C. After removing the primary antibodies, the cells were incubated in the dark with the corresponding secondary antibodies for 1 h. Subsequently, the cell nuclei were stained with DAPI. The cells were photographed under an inverted fluorescence microscope. Flow cytometry was performed using an ACEA FC500 flow cytometer (Beckman Coulter, Fullerton, CA, USA). The acquired data were analyzed in FlowJo to quantify CD206 and CD86 expression levels. Finally, the production of inflammation-associated cytokines, including TNF-α and IL-10, in RAW264.7 cells treated with different samples was analyzed using commercial ELISA kits according to the manufacturer's instructions.

1.4. Fabrication and characterization of functionalized hydrogels

First, 2 wt% HA-DOPA and 2 wt% Alg-PBA solutions were prepared at room temperature. Then HA-DOPA and Alg-PBA solutions were mixed at an equal volume ratio to obtain the precursor solution (HDAP), and the pH was adjusted to 8.5 by adding NaOH solution (0.1 M). TCM was added to the above HDAP precursor solution under continuous stirring to make the final concentration of 0.5 mg/mL. Finally, the mixed precursor solution was allowed to stand for 5 min at room temperature to obtain HDAP/TCM hydrogel. As a control, HDAP (without TCM) and HDAP/CM (with an equal amount of CM) hydrogels were prepared under the same synthesis conditions. Hydrogel formation was evaluated using the inverted bottle method.

The morphologies and microstructures of various materials were characterized by FE-SEM equipped with EDS. FTIR determined the phase structure and composition of multiple materials. A high-resolution microcomputed tomography system (micro-CT, SkyScan 1276, Bruker, Germany) was used to observe the 3D porous structure and analyze porosity and pore-size distribution. The rheological properties of the prepared hydrogels were tested using a rotational rheometer (TA Instruments, HAAKE Mars III). The mechanical properties were determined using a universal mechanical testing system (CMT6503, Shenzhen SANS Test Machine, China). For the degradation behavior, the initial weight of the freeze-dried hydrogel (W0) was recorded. The hydrogel was then immersed in PBS solution (pH=7.4) containing 1 U/mL of collagenases II and incubated at 37°C. At each time point, the hydrogel was removed, freeze-dried, and re-weighed (W1). The degradation rate was calculated using the formula: Degradation rate (%) = W0/W1 × 100%. To evaluate pH- and ROS-responsive degradation behavior, the HDAP/TCM hydrogel sample was immersed in Tris-HCl buffer (pH 5.5 or 7.4) with or without 1 mM H_2O_2. The degradation was quantified by measuring the weight change as mentioned above. For in vitro swelling experiments, the initial freeze-dried weight (M0) of each hydrogel sample was recorded. The samples

were immersed in simulated body fluid (SBF) solution (pH=7.4) at 37°C. At the scheduled time points, the samples were removed and reweighed (M1). The swelling ratio was calculated as: Swelling ratio = [(M0-M1)/M1] × 100%. To quantify Ca2+ release, the samples were soaked in Tris-HCl buffer (pH 7.4) with or without daily NIR irradiation (808 nm, 0.5 W/cm^2) for 5 min. The resulting solutions were analyzed using ICP-OES. To evaluate the release kinetics of TA from the hydrogel, hydrogel samples were placed in Tris-HCl buffer solution under different levels of acidic conditions (pH = 6.5 and 7.4) with or without H_2O_2 (1 mM). Additionally, the collected supernatant was analyzed using a UV-vis spectrophotometer, and the concentration of TA released from hydrogels was determined from the standard curve and the measured absorbance.

1.5. Injectability, adhesion, photothermal, and characterization of functionalized hydrogels

To demonstrate the injectable performance of the HDAP/TCM hydrogel, the composite was loaded into a syringe fitted with a 22G needle and extruded to pattern the letters “Hydrogel” as a visual validation. For systematic macroscopic evaluation of the self-healing potential, the hydrogel samples were gelled into tablet-like configurations and stained with distinct dyes to facilitate visualization. These dyed hydrogel tablets were then bisected, and the fragmented parts were reconnected after mutual exchange of their separated sections.

The in vitro antioxidant capacity of the composite hydrogels was assessed using DPPH and ABTS free radical scavenging assays, as previously described[2]. In brief, various hydrogel samples were added to the DPPH or ABTS reaction system and incubated in the dark for 20 min, with or without NIR irradiation (808 nm, 0.5 W/cm^2) for 5 min. Finally, the absorbance of each sample was measured using a microplate reader. To assess the photothermal properties of the composite microspheres, the samples were immersed in PBS and irradiated with an 808 nm NIR laser at a power density of 0.5 W/cm^2 for 10 min. During irradiation, temperature changes were monitored using an infrared thermal imaging camera (FLIR Systems, Inc., Wilsonville, OR). After determining the photothermal properties, the samples' temperature changes were further tested at various power densities. To assess the photothermal properties of the composite hydrogels, the samples were immersed in PBS solution and irradiated with an 808 nm NIR laser at a power density of 0.5 W/cm^2 for 10 min. The temperature changes in the hydrogel were recorded using an infrared thermal imaging camera. Additionally, the photothermal stability of these materials was recorded across five on/off cycles of NIR irradiation.

1.6. In vitro evaluation of osteogenic activity under oxidative stress conditions

The osteogenic capability of the hydrogel was evaluated using BMSCs under oxidative stress conditions, as previously reported[3]. Briefly, BMSCs were seeded into 24-well plates and incubated at 37°C with 5% CO_2. The cells were then treated with 500 μM H_2O_2 for 24 h and cocultured with the different hydrogel groups. For the HDAP/TCM+ group, the samples were exposed to the 808 nm NIR laser (0.5 W/cm^2) for 5 min daily. The BMSCs cultured in the H_2O_2-stimulated complete medium were set as the control group. After incubation for 48 h, CCK-8 assay, EdU staining, live/dead staining, cytoskeleton staining, DCFH-DA staining, and flow cytometry experiments were performed to investigate the cytoprotective effects under oxidative stress. Afterward, the mitochondrial membrane potential (MMP) of BMSCs was evaluated using the JC-1 MMP assay kit, in accordance with the provided instructions[4]. Meanwhile, the expression levels of oxidative stress-related genes in BMSCs were evaluated by qRT-PCR as described above. To evaluate osteogenic activity under oxidative stress, 500 μM H_2O_2 was added to the osteogenic induction medium as previously described. After 7 days of osteogenic induction, ALP staining and activity assay were performed using the same procedure described above. After 14 days, ARS and Von Kossa staining assays were performed to evaluate mineralization. Additionally, immunofluorescence staining and western blotting were used to examine the expression of osteogenesis-related proteins in BMSCs from all experimental groups. The effects of the hydrogels on the osteogenic markers of BMSCs at the molecular level were investigated using qRT-PCR after 7 days, as mentioned above. The expression levels of the target genes were quantified using the 2-ΔΔCT method, normalized to the reference gene GAPDH. Primers used in this study are listed in **Table S1**. The expression levels of osteogenesis-related proteins were determined by western blot analysis, as described in a previous study[5]. Briefly, the BMSCs after various treatments were collected and lysed in RIPA buffer on ice. The total protein content of the target protein was determined using the BCA method. The proteins were then separated by SDS-PAGE and transferred to polyvinylidene difluoride (PVDF) membranes. The membranes were incubated with specific primary antibodies overnight at 4°C. This was followed by incubation with HRP-conjugated secondary antibodies for 1 h. Protein bands were visualized using an enhanced chemiluminescence detection system (Tanon, Shanghai, China).

1.7. In vitro evaluation of angiogenic activity under oxidative stress conditions

The angiogenic capacity of the hydrogel was evaluated in HUVECs under oxidative stress conditions using previously reported methods[6]. Briefly, HUVECs were seeded into 24-well plates and incubated at 37°C with 5% CO_2. The cells were then treated with 500 μM H_2O_2 for 24 h and cocultured with the different hydrogel groups. For the HDAP/TCM+ group, the samples were exposed to the 808 nm NIR laser (0.5 W/cm^2) for 5 min daily.

HUVECs cultured in H_2O_2-stimulated complete medium served as the control group. To assess cell viability, survival, and apoptosis, CCK-8 assays, EdU staining, and flow cytometry were performed after 2 days. Additionally, cytoskeleton staining and DCFH-DA staining were performed as described above. Subsequently, the wound-healing assay, Transwell migration assay, and tube formation assay were performed to assess the angiogenic capacity of HUVECs under the oxidative stress conditions described above. For the wound healing assay, HUVECs were cocultured with various pre-gels for 24 h until they reached approximately 90% confluence. An artificial “scratch” area was created using a sterile pipette tip, and cell debris was gently removed by washing three times with PBS. After staining with crystal violet, the samples were observed and photographed under an inverted microscope at 0 and 24 h. For the Transwell migration assay, HUVECs were added to the upper chamber of a 24-well plate at a density of 5×10^4 cells/mL, while 500 μL of complete DMEM containing various pre-gels was added to the lower chamber. After 24 h of incubation, the cells on the lower surface of the membrane were fixed with 4% paraformaldehyde, then stained with 1% crystal violet for 15 min. The migrated cells were photographed using an optical microscope. For the tube formation assay, HUVECs were seeded in 24-well plates pre-coated with Matrigel and cultured in complete medium supplemented with various pre-gels for 6 h. The cells were stained with Calcein-AM for 15 min, and the images were captured using an inverted fluorescence microscope. To further evaluate the angiogenic potential of HUVECs after different treatments, qRT-PCR, immunofluorescence staining, and western blotting were performed on day 7 as described above. The primer sequences for the relevant genes are displayed in **Table S1**.

1.8. In vitro evaluation of macrophage reprogramming, anti-inflammatory, and osteoimmunomodulatory functions

To measure intracellular ROS, RAW264.7 cells were cocultured with H_2O_2 (500 μM) and then treated with various hydrogels for 24 h, with or without NIR irradiation as described above. Subsequently, the cells were stained with 10 μM DCFH-DA for 30 min in the dark according to the manufacturer’s instructions. The stained cells were photographed and observed using an inverted fluorescence microscope. Meanwhile, the cytoprotective effects of different treatments were evaluated using CCK-8, EdU staining, and live/dead staining at specific time points. To evaluate anti-inflammatory and immunomodulatory functions, RAW264.7 cells were stimulated with H_2O_2 (500 μM) and then treated with various hydrogels for 3 days, with or without NIR irradiation as described above. Subsequently, the anti-inflammatory activity was investigated by flow cytometry using CD86 as a marker for M1 (inflammatory) macrophages and CD206 as a marker for M2 (anti-inflammatory) macrophages. To comprehensively evaluate the immunomodulatory effects, an immunofluorescence staining assay was performed to assess polarization

markers (F4/80, CD86, and CD206) in M0/M1/M2 cells. Western blotting was used to detect TNF-α and IL-10 expression, with GAPDH as the reference gene. In addition, qRT-PCR was used to detect mRNA expression, and the primers are shown in **Table S1**.

To investigate whether osteogenic differentiation and mineralization of BMSCs are affected by hydrogel-regulated macrophage polarization, we collected supernatants from extracts prepared using different matrices after coculturing with LPS-treated RAW264.7 cells for 48 h. The collected supernatant was centrifuged and filtered. After filtration, the supernatant was mixed with an osteogenic induction medium at a 1:1 ratio to produce a conditioned medium. After 7 days of incubation, ALP staining and activity assay were performed as mentioned above. The total protein content was determined using a BCA protein quantification kit to standardize ALP. After 14 days of incubation, calcium mineralization was determined by ARS staining. In addition, immunofluorescence staining and qRT-PCR were used to evaluate osteogenic marker expression levels. The primer sequences used are shown in **Table S1**.

To elucidate the mechanism by which the HDAP/TCM+ influences macrophage polarization and tissue regeneration, LPS-treated RAW264.7 macrophages were cocultured with HDAP/TCM plus mild photothermal stimulation for 3 days. TRIzol reagent was used to extract total RNA from cells according to the manufacturer's instructions. Next, RNA sequencing (RNA-seq) was performed by Frasergen Bioinformatics Co., Ltd. Statistical significance was set at $P < 0.05$, and fold changes of > 2 or < 0.5 were used to determine differentially expressed genes (DEGs). These DEGs were then subjected to the Gene Ontology (GO) and Kyoto Encyclopedia of Genes and Genomes (KEGG) databases for functional and signaling pathway enrichment analyses. Differences between the control and HDAP/TCM+ groups were analyzed using gene set enrichment analysis (GSEA) across predefined gene sets.

1.9. In vivo subcutaneous implantation

All animal procedures were approved by the Animal Care and Use Committee of Wuhan University, and the protocols complied with the Guide for the Care and Use of Laboratory Animals. A subcutaneous implantation experiment was carried out on male Sprague-Dawley (SD) rats (6-week-old). Under general anesthesia and sterile conditions, the hydrogel discs (5 mm in diameter, 1 mm in height) were implanted subcutaneously into the dorsal region of each rat. For the HDAP/TCM+ group, the implanted areas were exposed to 808 nm NIR irradiation (0.5 W/cm^2) for 5 min 24 h after surgery. The irradiation procedure was performed every 2 days to maintain the temperature at 42 ± 1°C, followed by a natural cooling period. Two weeks after subcutaneous transplantation, the rats were sacrificed, and the implanted hydrogels with the surrounding tissue were removed and fixed in 4% paraformaldehyde. The samples were subsequently embedded in paraffin and

sectioned at 5 μm for histological analysis, including hematoxylin and eosin (H&E) staining, immunohistochemistry (MPO, CD44, and CD90), and immunofluorescence (iNOS, CD206, Runx2, and CD31), in accordance with standard or published protocols. Moreover, ROS levels in the hydrogels and surrounding tissue were evaluated using dihydroethidium (DHE) staining of frozen sections from collected samples. The remaining portion of the tissue was immediately frozen in liquid nitrogen after collection and then stored at -80°C for ELISA experiments. To detect inflammation-related gene expression, the collected samples were homogenized, and total RNA was extracted for reverse transcription. Then, qRT-PCR was performed using ChamQ SYBR qPCR Master Mix according to the manufacturer's instructions. The primer sequences are listed in **Table S1**. To assess systemic biocompatibility, major organs, including the heart, liver, spleen, lung, and kidney, were collected from rats in each treatment group after 8 weeks of in vivo implantation. The harvested tissues were fixed in 4% paraformaldehyde for 24 h, dehydrated, embedded in paraffin, and sectioned at 5 μm. The sections were stained with H&E for histological assessment according to standard procedures. Meanwhile, blood biochemical parameters, including alanine transaminase (ALT), aspartate transaminase (AST), blood urea nitrogen (BUN), and creatinine (CR), were assessed after various treatments.

1.10. Evaluation of osteoporotic bone defect healing in rats

Following the previously reported procedure[7], bilateral ovariectomy was used to induce an osteoporosis model in female SD rats (6-week-old). After anesthesia with 3% pentobarbital sodium, the bilateral ovaries of female rats were removed. After 12 weeks, the femurs were collected for micro-CT analysis and histological staining to evaluate bone loss in ovariectomized (OVX) rats. Additionally, immunohistochemistry and immunofluorescence are used to assess inflammation, oxidative stress, and osteoclast activity and function. Once the OVX model was successfully established, a total of forty-five SD rats were randomly divided into five groups: control, HDAP, HDAP/CM, HDAP/TCM, and HDAP/TCM+ (receiving daily periodic 808 nm NIR laser irradiation for 5 min at a power density of 0.5 W/cm^2). After anesthesia with isoflurane gas inhalation, bilateral cranial defects (Φ = 5 mm) were created in OVX rats using a dental low-speed ring drill. Various hydrogels (50 μL) were injected into the defects, while the rats without implanted materials served as the control group. In the HDAP/TCM+ group, the photothermal effect was monitored with an infrared thermal imaging camera. At 6 and 12 weeks post-surgery, rats were euthanized, and cranium specimens were harvested and fixed with 4% paraformaldehyde at 4°C overnight. These specimens were then scanned using micro-CT at a resolution of 6.5 μm. Subsequently, 3D reconstruction was conducted, and bone morphometric parameters, including bone mineral density (BMD), bone tissue volume/total tissue volume (BV/TV), trabecular thickness (Tb.Th), and trabecular separation (Tb.Sp),

were measured and analyzed using micro-CT analysis software. Following micro-CT analysis, histological and immunofluorescence staining were performed to further investigate therapeutic effects across different treatment groups. The calvarium samples were decalcified in ethylenediaminetetraacetic acid (EDTA), dehydrated, embedded in paraffin, and sectioned at 5 μm. Sections were stained with H&E and Masson's trichrome (MST) to observe tissue structure and collagen deposition in the defect areas. The stained sections were examined under a light microscope to evaluate bone regeneration and ECM remodeling. Meanwhile, immunofluorescence staining was performed to assess the expression of osteogenesis- and osteoclastogenesis-related markers in the post-surgery samples, including Runx2, OPN, TRAP, and NFATc1. To evaluate early inflammation/immune responses, as well as tissue regeneration, immunohistochemistry and immunofluorescence staining were performed at 2 weeks after implantation. For immunofluorescence staining of DHE, iNOS, CD206, Runx2, and CD31, fixed, frozen tissue sections were stained with the corresponding antibodies according to the manufacturer's instructions. The sections were incubated with primary antibodies against TNF-α, IL-10, HO-1, BMP-2, and VEGF, followed by incubation with horseradish peroxidase (HRP)-conjugated secondary antibodies.

1.11. Statistical analysis

In this study, the experimental data are presented as mean ± standard deviation (mean ± SD). Statistical analysis was conducted using Origin 2018 software (Origin Lab Corporation, USA) by one-way ANOVA with Tukey's test. Data with abnormal distribution or heterogeneity of variance were analyzed by the Mann-Whitney U test and Kruskal-Wallis's nonparametric test. The values were considered significant at p^* or $p^{\#}$, with a p value < 0.05, and highly significant at p^{**} or $p^{\#\#}$, with a p value < 0.01.

Supplementary figures and tables

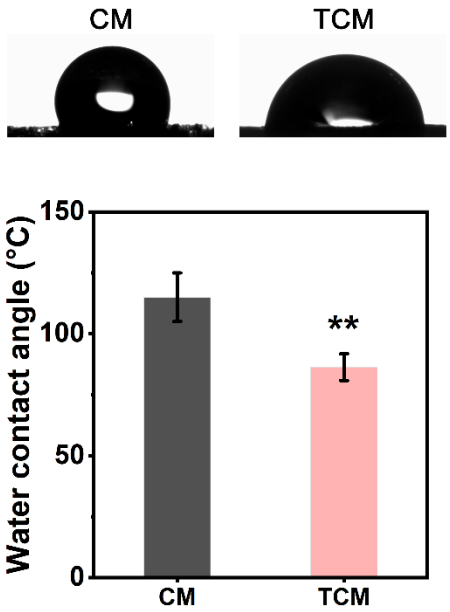

Figure S1. Water contact angle measurement. Data are expressed as mean ± SD (n=3). Significant differences compared to the CM group are indicated by *P < 0.05 and **P < 0.01.

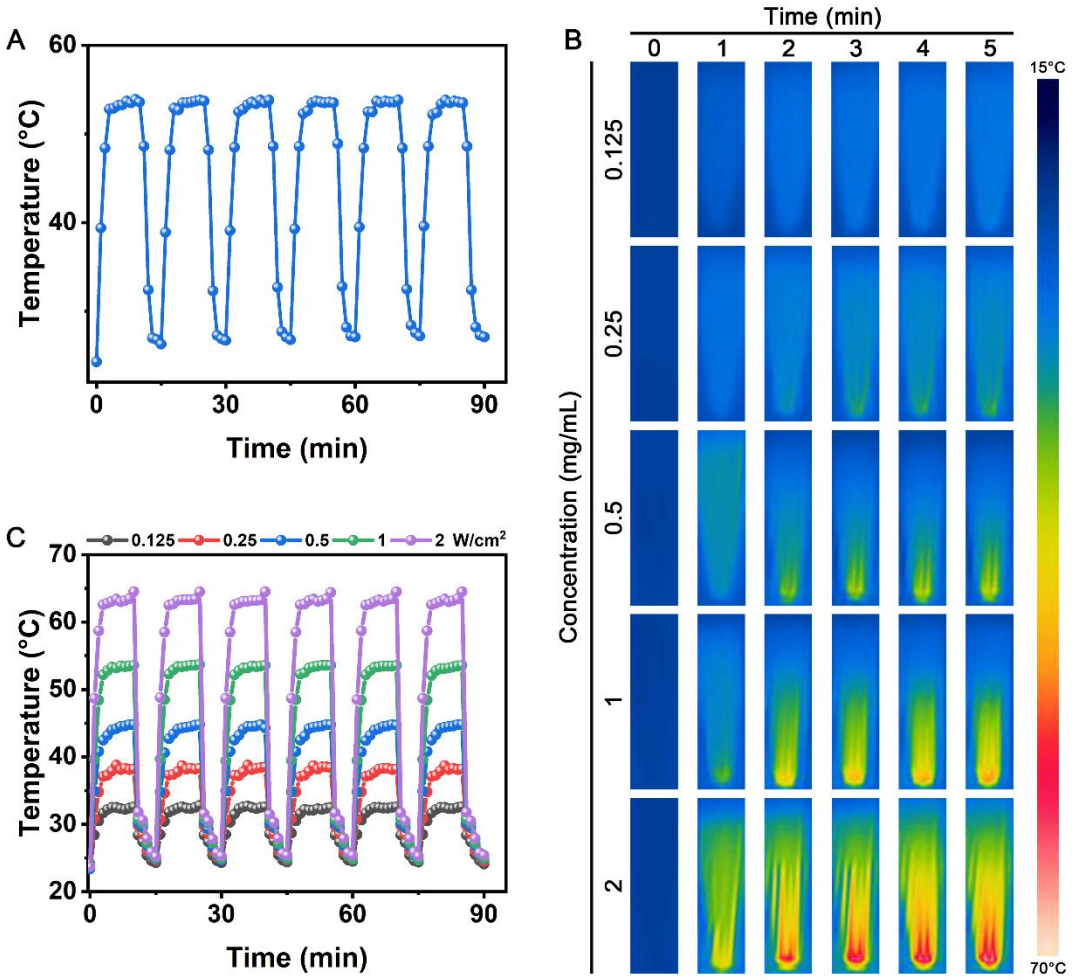

Figure S2. (A) Temperature cycling profile of TCM solution under six cycles of 808 nm laser irradiation at 0.5 W/cm^2. **(B-C)** Photothermal heating curves of TCM solution under different laser power densities and related real-time infrared thermal images.

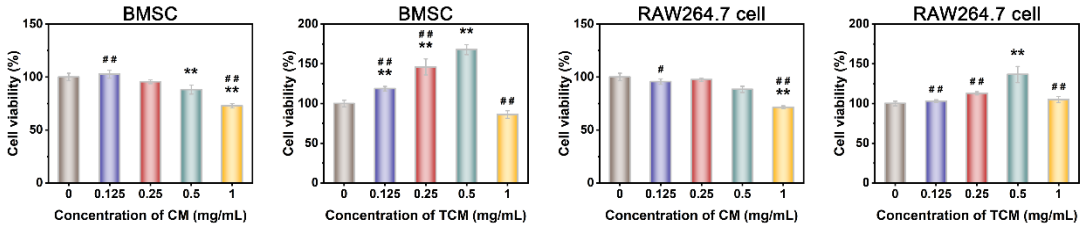

Figure S3. CCK-8 assay of BMSCs and RAW264.7 cells incubated with different microspheres at various concentrations for 3 days. Data are expressed as mean ± SD (n=3). Significant differences compared to the 0 mg/mL-treated group are indicated by *P < 0.05 and **P < 0.01. Significant differences compared to the 0.5 mg/mL-treated group are indicated by $^{\#}$P < 0.05 and $^{\#\#}$P < 0.01.

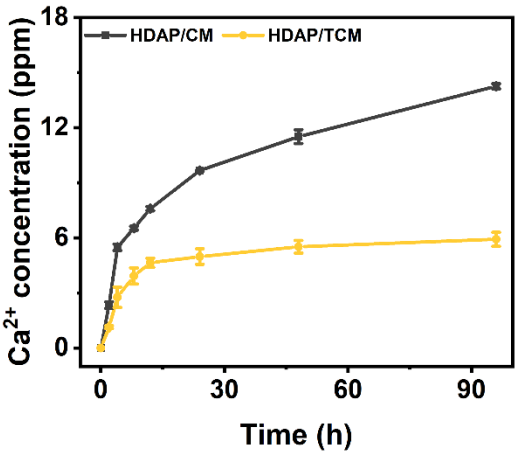

Figure S4. ^{1}H NMR spectra of Alg and Alg-PBA.

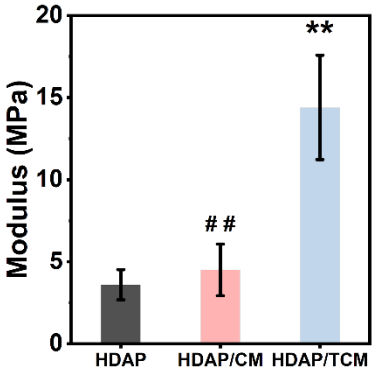

Figure S5. Compressive modulus of various hydrogels. Data are expressed as mean ± SD (n=3). Significant differences compared to the HDAP group are indicated by *P < 0.05 and **P < 0.01. Significant differences compared to the HDAP/TCM group are indicated by $^{\#}$P < 0.05 and $^{\#\#}$P < 0.01.

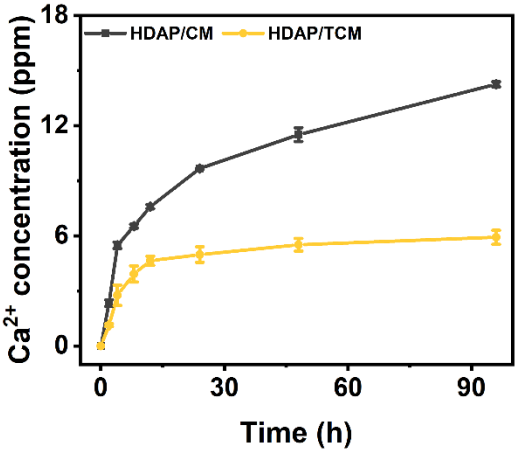

Figure S6. Cumulative release profiles of Ca^{2+} from various microspheres. Data are expressed as mean ± SD (n=3).

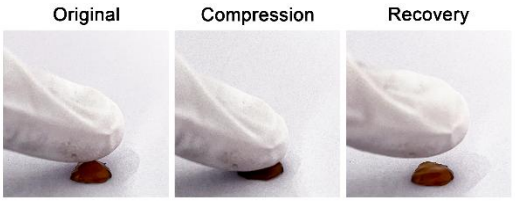

Figure S7. Macroscopic mechanical behavior of the HDAP/TCM hydrogel.

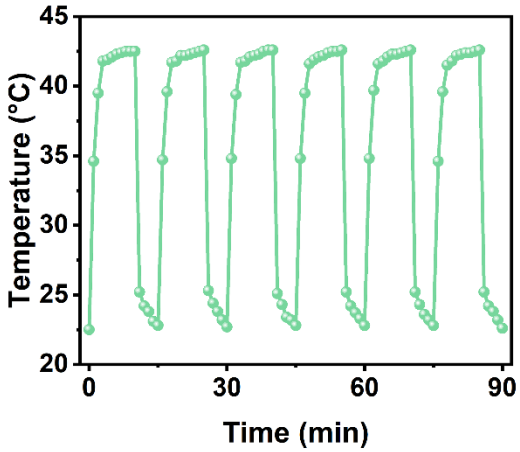

Figure S8. Temperature cycling profile of HDAP/TCM hydrogel under six cycles of 808 nm laser irradiation at 0.5 W/cm^2.

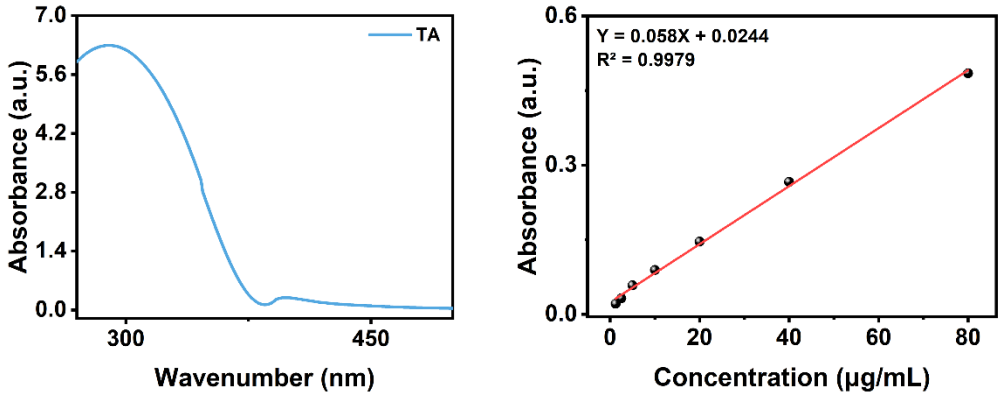

Figure S9. The UV-vis absorbance spectra and standard curve of TA.

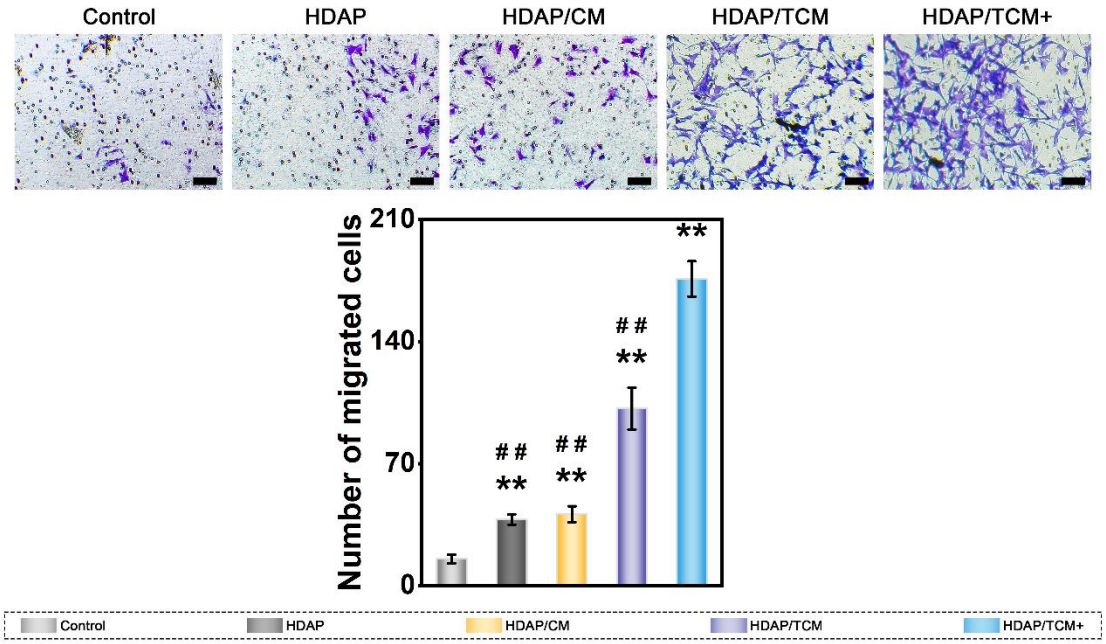

Figure S10. Representative images and corresponding quantitative analysis of the BMSC Transwell migration assay in each group. Data are expressed as mean ± SD (n=3). Significant differences compared to the Control group are indicated by *P < 0.05 and **P < 0.01. Significant differences compared to the HDAP/TCM+ group are indicated by $^{\#}$P < 0.05 and $^{\#\#}$P < 0.01.

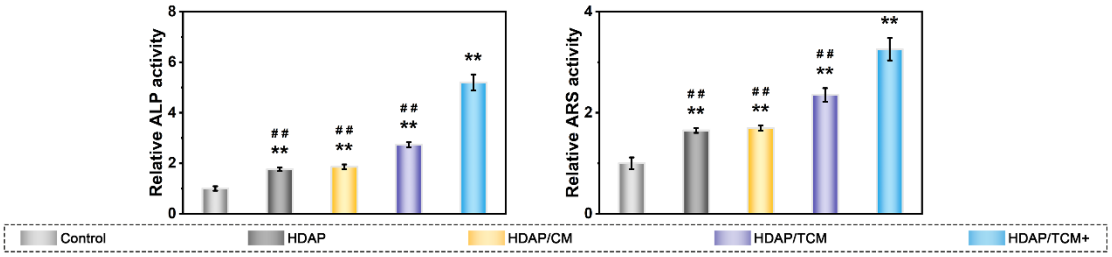

Figure S11. Quantitative analysis of ALP staining and ALP activity in each group. Data are expressed as mean ± SD (n=3). Significant differences compared to the Control group are indicated by *P < 0.05 and **P < 0.01. Significant differences compared to the HDAP/TCM+ group are indicated by $^{\#}$P < 0.05 and $^{\#\#}$P < 0.01.

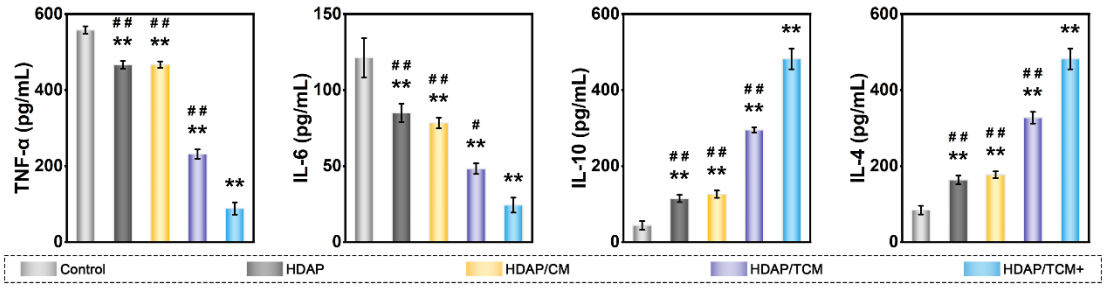

Figure S12. ELISA quantification of inflammatory mediators in the cell culture medium of RAW264.7 cells after different treatments. Data are expressed as mean ± SD (n=3). Significant differences compared to the Control group are indicated by *P < 0.05 and **P < 0.01. Significant differences compared to the HDAP/TCM+ group are indicated by $^{\#}$P < 0.05 and $^{\#\#}$P < 0.01.

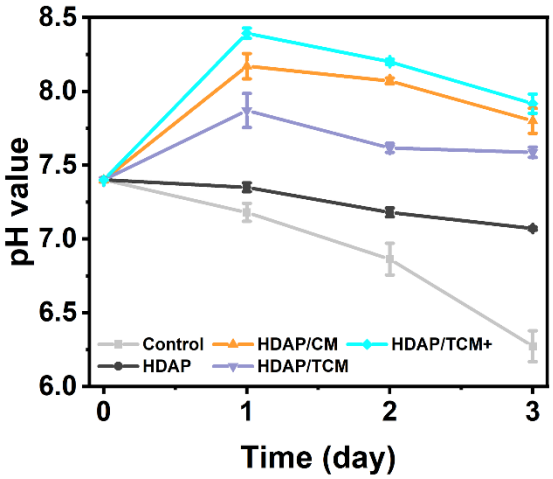

Figure S13. The effect of different hydrogel treatments on the pH value in neutral solution conditions. Data are expressed as mean ± SD (n=3).

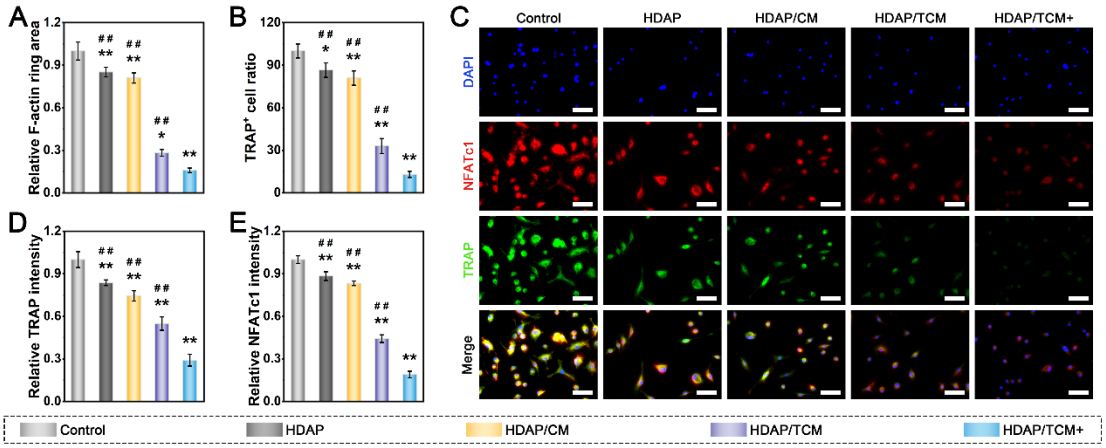

Figure S14. (A-B) Quantitative analysis of F-actin ring assay and TRAP staining. **(C-E)** Immunofluorescence staining and quantitative analysis of TRAP and NFATc1 in BMMs after different treatments. Scale bar: 50 μm. Data are expressed as mean ± SD (n=3). Significant differences compared to the Control group are indicated by *P < 0.05 and **P < 0.01. Significant differences compared to the HDAP/TCM+ group are indicated by $^{\#}$P < 0.05 and $^{\#\#}$P < 0.01.

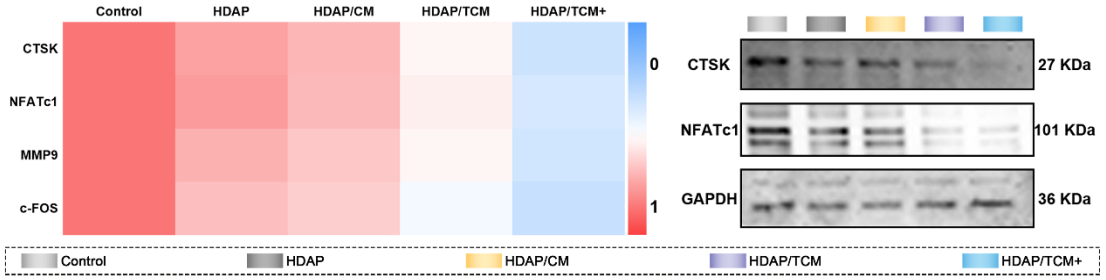

Figure S15. Relative expression levels of osteoclastogenesis-related markers in BMMs detected by qRT-PCR and western blot analysis. Data are expressed as mean ± SD (n=3).

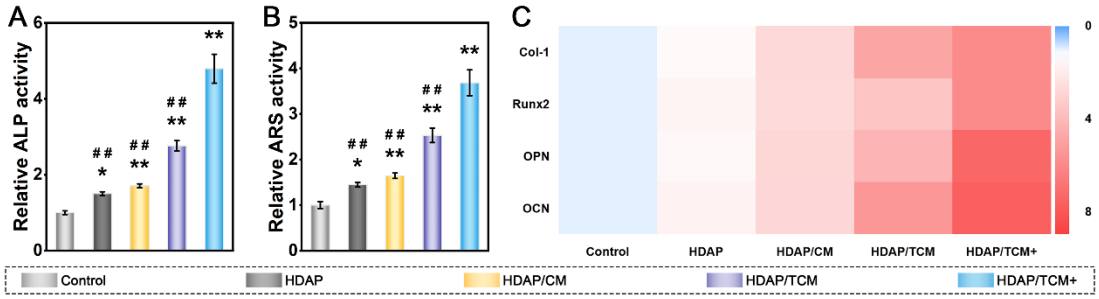

Figure S16. (A-B) Quantitative analysis of ALP activity and ARS staining. **(C)** Heatmap of osteogenesis-related gene expression. Data are expressed as mean ± SD (n=3). Significant differences compared to the Control group are indicated by *P < 0.05 and **P < 0.01. Significant differences compared to the HDAP/TCM+ group are indicated by $^{\#}$P < 0.05 and $^{\#\#}$P < 0.01.

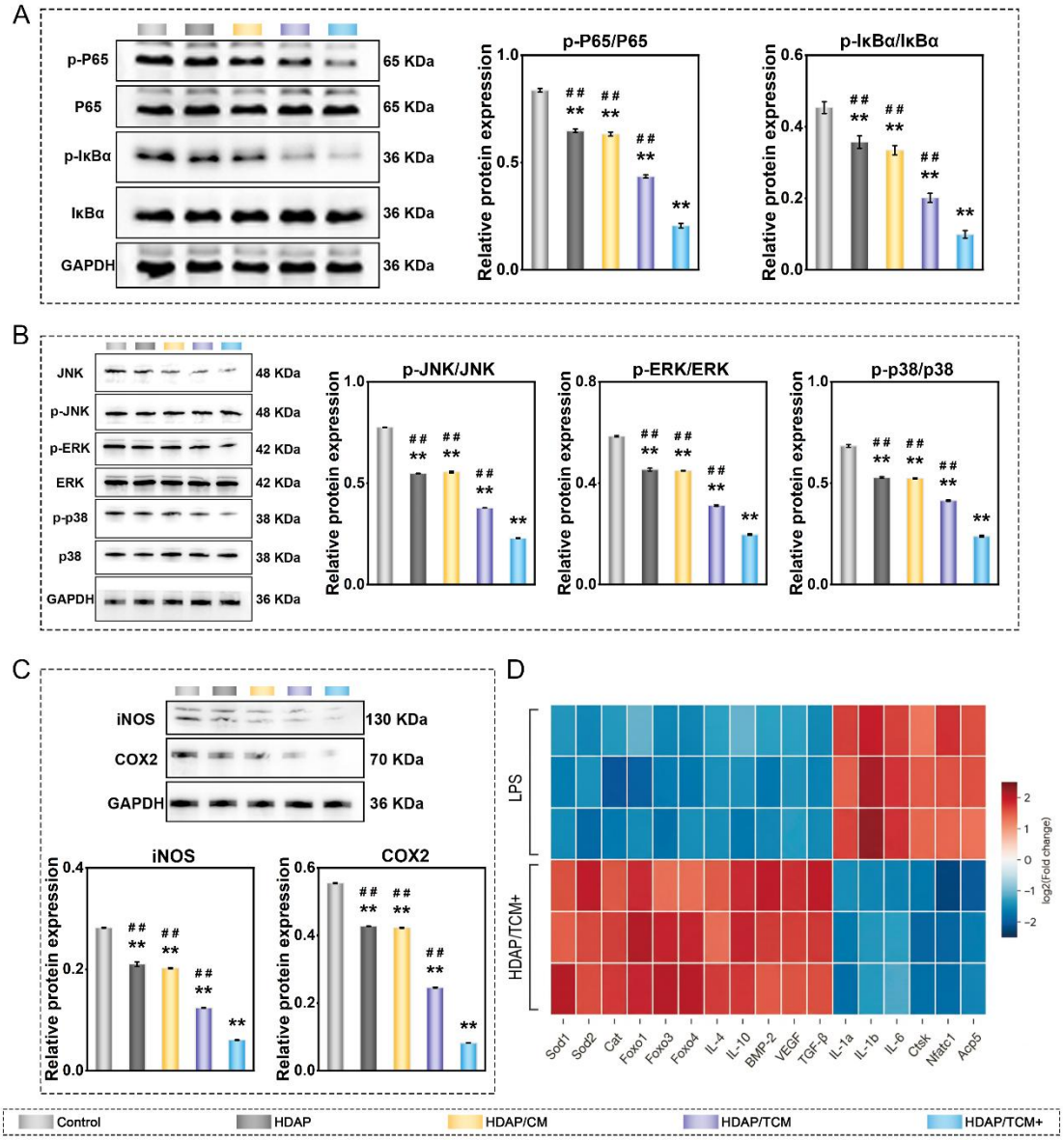

Figure S17. (A) Western blot analysis of NF-κB signaling pathway-related protein expression in RAW264.7 cells after different treatments. **(B)** Western blot analysis of MAPK signaling pathway-related protein expression in RAW264.7 cells after different treatments. **(C)** Western blot analysis of TNF signaling pathway-related protein expression in RAW264.7 cells after different treatments. **(D)** Heatmap analysis of DEGs involved in antioxidative stress, tissue repair, osteoclastogenesis, and inflammation. Data are expressed as mean ± SD (n=3). Significant differences compared to the Control group are indicated by *P < 0.05 and **P < 0.01. Significant differences compared to the HDAP/TCM+ group are indicated by $^{\#}$P < 0.05 and $^{\#\#}$P < 0.01.

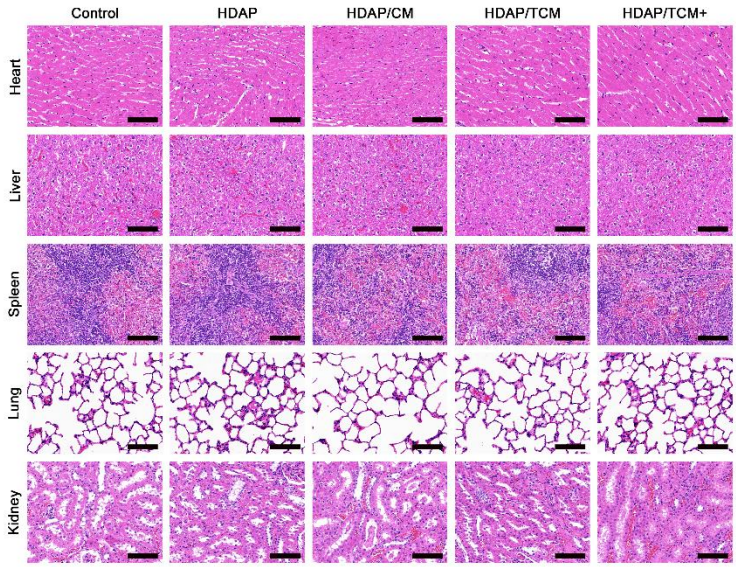

Figure S18. H&E staining of major organs, including the heart, liver, spleen, lung, and kidney, after 8 weeks. Scale bar: 100 μm.

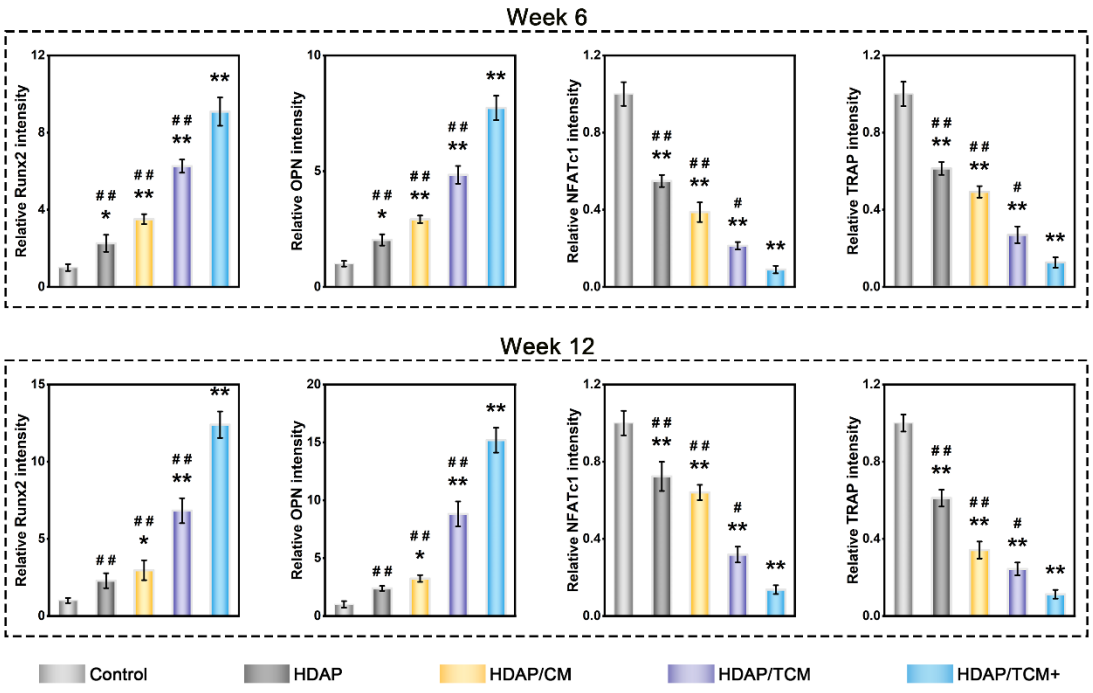

Figure S19. Quantitative analysis of immunofluorescence staining of collected samples after 6 and 12 weeks. Data are expressed as mean ± SD (n=3). Significant differences compared to the Control group are indicated by *P < 0.05 and **P < 0.01. Significant differences compared to the HDAP/TCM+ group are indicated by $^{\#}$P < 0.05 and $^{\#\#}$P < 0.01.

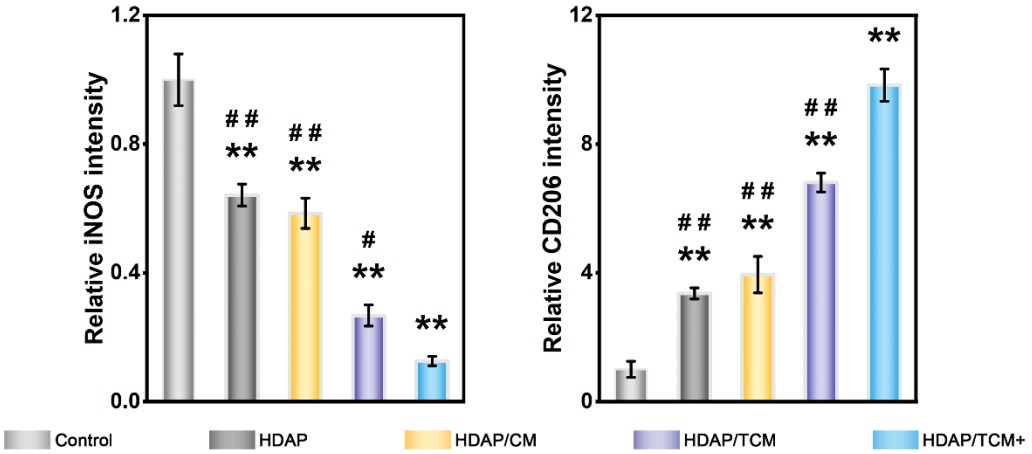

Figure S20. Quantitative analysis of immunofluorescence staining of collected samples after 2 weeks. Data are expressed as mean ± SD (n=3). Significant differences compared to the Control group are indicated by *P < 0.05 and **P < 0.01. Significant differences compared to the HDAP/TCM+ group are indicated by $^{\#}$P < 0.05 and $^{\#\#}$P < 0.01.

Table S1.

Genes	Primers (F, forward; R, reverse; 5'-3')
Mouse-GADPH	F: TCAACGGCACAGTCAAGG
	R: TTAGTGGGGTCTCGCTCC
Mouse-Runx2	F: CATCCCAGTATGAGAGTAGGTGT
	R: GCTCAGATAGGAGGGGTAAGAC
Mouse-Col-1	F: CTGACTGGAAGAGCGGAGAG
	R: CGGCTGAGTAGGGAACACAC
Mouse-OPN	F: TCTGAGGGACTAACTACGACCAT
	R: TGGAAGAGTTTCTTGCTTAAAGTC
Mouse-OCN	F: TTCTGCTCACTCTGCTGACCC
	R: CTGATAGCTCGTCACAAGCAGG
Mouse-HSP47	F: GCCGAGGTGAAGAAACCCC
	R: CATCGCCTGATATAGGCTGAAG
Mouse-HSP70	F: CAGCGAGGCTGACAAGAAGA
	R: GAGGCTCCTTTCGGCGG
Mouse-TNF-α	F: CAGGCGGTGCCTATGTCTC

	R: CGATCACCCCGAAGTTCAGTAG
Mouse-IL-6	F: GAGACCACTGGGGAGAATGC
	R: TTGCCAGGTGGGTAAAGTGG
Mouse-iNOS	F: GAATCTTGGAGCGAGTTG
	R: CCAGGAAGTAGGTGAGGG
Mouse-CD86	F: ATGGGCTCGTATGATTGT
	R: TCTTAGGTTTCGGGTGAC
Mouse-TGF-β	F: ACCGCAACAACGCCATCT
	R: GGGCACTGCTTCCCGAAT
Mouse-IL-10	F: TTTCAAACAAAGGACCAG
	R: GGATCATTTCCGATAAGG
Mouse-Arg-1	F: AAGACAGCAGAGGAGGTG
	R: AGTCAGTCCCTGGCTTA
Mouse-CD206	F: GCAAGTGATTTGGAGGCT
	R: ATAGGAAACGGGAGAACC
Mouse-SOD2	F: CAGACCTGCCTTACGACTATGG
	R: CTCGGTGGCGTTGAGATTGTT
Mouse-CAT	F: AGCGACCAGATGAAGCAGTG
	R: TCCGCTCTCTGTCAAAGTGTG
Mouse-GPX1	F: AGTCCACCGTGTATGCCTTCT
	R: GAGACGCGACATTCTCAATGA
Mouse-CTSK	F: GCACCCTTAGTCTTCCGCTC
	R: GGTCATATAGCCGCCTCCAC
Mouse-NFATc1	F: TATATGAGCCCATCCTTGCCT
	R: GGCTGCCTTCCGTCTCATAG
Mouse-c-FOS	F: TTGAGCGATCATCCCGGTC
	R: GCGTGAGTCCATACTGGCAAG
Mouse-MMP9	F: CTGGACAGCCAGACACTAAAG
	R: CTCGCGGCAAGTCTTCAGAG

Rat-GAPDH	F: CTCCCATTCTTCCACCTTTG
	R: TGGTCCAGGGTTTCTTACT
Rat-iNOS	F: GAGACGCACAGGCAGAGGTTG
	R: AGCAGGCACACGCAATGATGG
Rat-CD86	F: CGAACACTATTTGGGCGCAG
	R: CAAACTGGGGCTGCGAAAAA
Rat- CD206	F: GACGGACGAGGAGTTCATTATACR
	R: GTTGGAGAGATAGGCACAGAAG
Rat-Arg-1	F: GGACATCGTGTACATCGGCT
	R: TTTGCTGTGATGCCCCAGAT
Human-GAPDH	F: CATCATCCCTGCCTCTACTGG
	R: GTGGGTGTCGCTGTTGAAGTC
Human-VEGF	F: TATGCGGATCAAACCTCACCA
	R: CACAGGGATTTTTCTTGTCTTGCT
Human-HIF-1α	F: ATCCATGTGACCATGAGGAAAT
	R: CTCGGCTAGTTAGGGTACACTT
Human-Ang-1	F: CAGGAGGATGGTGGTTTG
	R: GCCCTTTGAAGTAGTGCC
Human-eNOS	F: ATGTTTGTCTGCGGCGATGT
	R: GTGCGTATGCGGCTTGTC

References

1. Wang T, Wen M, Li N, Zhang L, Xue Y, Shang L: **Marine-Derived Nanozyme-Crosslinked Self-Adaptive Hydrogels for Programmed Regulating the Regeneration Process.** *Advanced Functional Materials* 2024, **34:**2405257.
2. Yang Z, Zhu Y, Cheng J, Chen Y, Wu P, Liu X, Cai L, Du L, Wu M: **Polyphenol-Derived Nanoarmor-Functionalized Photothermal Hydrogel Platform for Programmed Modulation of the Regenerative Microenvironment and Bone Defect Healing.** *Small* 2025**:**e10733.

3. Fu X, Luo Z, Guo Y, Meng W, Jin S, Chen J, Cai Y, Luo Z, Huang C, Chen A, et al: **Microenvironment-responsive multifunctional enzyme-linked hydrogel for diabetic bone defect regeneration.** *Nat Commun* 2025, **16:**10275.
4. Rui M, Mao J, Wu H, Hui Y, Shen H, Yang Y, Ma T, Ren K, Wang J, Cui W, et al: **Implantable Multifunctional Micro-Oxygen Reservoir System for Promoting Vascular-Osteogenesis via Remodeling Regenerative Microenvironment.** *Adv Sci (Weinh)* 2025, **12:**e2409636.
5. Yuan B, Peng H, Wang Y, Li J, Zhang Y, Chen Z, Li K, Tu C, Zhang K, Zhu X, et al: **Micro/Nanobiomimetic Iron-Based Scaffold Induces Vascularized Bone Regeneration To Repair Large Segmental Bone Defect in Load-Bearing Sites.** *ACS Nano* 2025, **19:**6840-6857.
6. Jiang J, Cai C, Li S, Xiong Y, Liu C, Shu Z, Yang J, Zheng M, Tang T, Liu W, et al: **Triple-effect strategy with taxifolin-whitlockite nanoparticles embedded hydrogel for osteoporotic bone defect repair and bone homeostasis modulation.** *Chemical Engineering Journal* 2025, **515:**163133.